

Nanoscale

Accepted Manuscript



This is an *Accepted Manuscript*, which has been through the Royal Society of Chemistry peer review process and has been accepted for publication.

Accepted Manuscripts are published online shortly after acceptance, before technical editing, formatting and proof reading. Using this free service, authors can make their results available to the community, in citable form, before we publish the edited article. We will replace this *Accepted Manuscript* with the edited and formatted *Advance Article* as soon as it is available.

You can find more information about *Accepted Manuscripts* in the [Information for Authors](#).

Please note that technical editing may introduce minor changes to the text and/or graphics, which may alter content. The journal's standard [Terms & Conditions](#) and the [Ethical guidelines](#) still apply. In no event shall the Royal Society of Chemistry be held responsible for any errors or omissions in this *Accepted Manuscript* or any consequences arising from the use of any information it contains.



Journal Name

ARTICLE

Fluorescent Nanoparticles Based on AIE Fluorogens for Bioimaging

Lulin Yan, Yan Zhang, Bin Xu* and Wenjing Tian*

Received 00th January 20xx,
Accepted 00th January 20xx

DOI: 10.1039/x0xx00000x

www.rsc.org/

Fluorescent nanoparticles (FNPs) have recently attracted increasing attention in the biomedical field because of their unique optical properties, easy fabrication and outstanding performance as imaging. Compared with conventional molecular probes including small organic dyes and fluorescent proteins, FNPs based on aggregation-induced emission (AIE) fluorogens have shown significant advantages in tunable emission and brightness, good biocompatibility, superb photo- and physical stability, potential biodegradability and facile surface functionalization. In this review, we summarize the latest advances in the development of fluorescent nanoparticles based on AIE fluorogens including polymer nanoparticles and silica nanoparticles over the past few years, and the various biomedical applications based on these fluorescent nanoparticles are also elaborated.

1. Introduction

Biological imaging (bioimaging) has become a powerful tool in biological research today because it offers a unique approach to visualize the morphological details of cells¹. Fluorescence imaging is one of the most powerful bioimaging techniques for real-time, noninvasive monitoring of biomolecules of interest in their native environments with high spatial and temporal resolution, and it is instrumental for revealing the fundamental insights into the production, localization, trafficking, and biological roles of biomolecules in complex living systems²⁻⁴. The development of fluorescent probes has facilitated the recent significant advances in cell biology and medical diagnostic imaging²⁻⁶. Over the past decades, a variety of fluorescent probes, such as semiconductor quantum dots, fluorescent carbon dots, Ln ion doped nanomaterials, photoluminescent silicon nanoparticles, metallic nanoclusters, organic small molecules and organic fluorescent nanoparticles have been synthesized and extensively investigated for biological applications⁶⁻¹⁵.

With the advantages of various unique optical and electronic properties, easy surface functionalization, fluorescent nanoparticles (FNPs) would be developed into new tools for bioimaging, diagnostics, drug delivery and therapy.^{16,17} Ideally, FNPs should have excellent dispersibility and stability, high targeting selectivity and good biocompatibility. Furthermore, the abilities of nanomaterials to accommodate multiple functional groups, such as targeting biomolecules, drugs, and genes, allow them to realize not only the detection of the structures and functioning of subcellular organelles and biomolecules, but also the targeted imaging and treatment of various cancers. Fabrications of colloidal nanoparticles with

well-controlled size- and shape-distributions, well-defined surface chemistry, and unique optical and electronic properties are the basis of all such biological applications of nanomaterials. The large surface to volume ratios of nanomaterials and their surface modifications using various chemical and bioconjugate reactions have moved the interface among chemistry, materials science and biology towards biomedical science.¹⁸ To date, a variety of organic fluorescent probes based on inorganic and organic nanomaterials and organic – inorganic hybrid systems have been developed for in vitro /in vivo sensing and imaging.¹⁹⁻²⁵

At present, the species of the organic small molecule fluorescent materials are the most abundant²⁶. With strong fluorescence in solution, these small organic molecules fluorescent materials always have weak emission or no emission at high concentration or in the aggregation, which was also called the aggregation-caused quenching (ACQ) effect²⁷. This phenomenon is very common for traditional dyes, due to π - π stacking between rigid planes and other non-radiative pathways, which will make the fluorescence intensity decreased²⁸. Fluorescence output of a bioconjugate is often limited by the degree of labeling (DL) or the number of fluorescent labels that are attached to a biopolymer chain.²⁹ Although more fluorogens can be loaded onto microspheres of synthetic polymers through elaborate control, the ACQ problem still persists, hampering the fabrication of highly emissive polymer beads. Recently, a new category of fluorogens with the opposite characteristics to the ACQ, aggregation-induced emission (AIE), has been developed.³⁰ AIE fluorogens are non-emissive in dilute solutions while are induced to emit intense fluorescence in aggregates. Since the first AIE fluorogens, 1-methyl-1,2,3,4,5-pentaphenylsilole, was reported by Tang's group³¹, many AIE fluorogens have been developed by various research groups, such as tetraphenylethene (TPE)³¹⁻³⁴, siloles³⁵⁻³⁷, distyrylanthracene (DSA)³⁸⁻⁴⁷, cyano-substituted diarylethene derivatives^{48,49}.

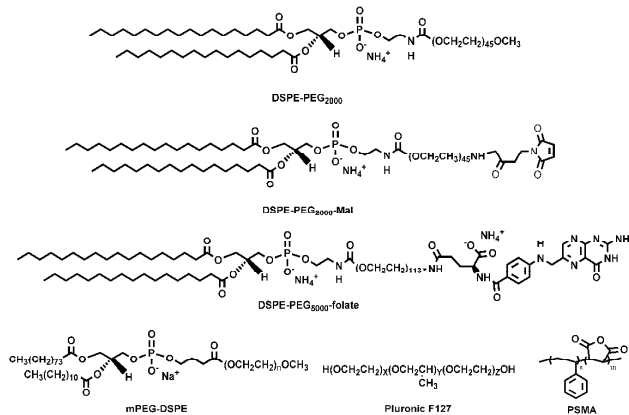
State Key Lab of Supramolecular Structure and Materials, Jilin University, Changchun, 130012, China. E-mail: xubin@jlu.edu.cn; wjtian@jlu.edu.cn

Restricted intramolecular rotation has been suggested as one of the possible mechanisms for the AIE phenomenon, considering that intramolecular rotations can drastically affect the radiative/non-radiative recombination processes of the excited state. Since the AIE effect allows a higher concentration of fluorophores to be loaded in FNPs, it makes the AIE-based FNPs more emissive and stronger photobleaching resistance.

In this review, we focus on the latest advances in the development of fluorescent nanoparticles based on AIE fluorogens for fluorescence bioimaging. Here, we classified fluorescent nanoparticles based on AIE fluorogens into three types. The first part covers the most widely studied physical cladding AIE fluorogens fluorescent nanoparticles, in which the AIE fluorogens are encapsulated into the polymer matrix. We present a number of amphiphilic polymer served as encapsulation matrix, which show various topology and fluorescent properties of the FNPs. The second part is focused on the covalent AIE fluorogens copolymer fluorescent nanoparticles. We summarize the mainly chemical reactions, which used to fix AIE fluorogens to the bioconjugate or polymerize to copolymer. The last part shows the recent development of fluorescent silica nanoparticles based on AIE fluorogens, such as encapsulated AIE fluorogens silica nanoparticles and covalent binding AIE fluorogens silica nanoparticles. Furthermore, various biological applications based on these AIE-based FNPs are elaborated and highlighted due to their attractive advantages as multifunctional platforms of imaging, targeting and delivery.

2. Physical cladding AIE fluorogens fluorescent nanoparticles

2.1 DSPE-PEG encapsulated nanoparticles



Scheme 1. Chemical structures of DSPE-PEG₂₀₀₀, DSPE-PEG₂₀₀₀-Mal, DSPE-PEG₅₀₀₀-folate, mPEG-DSPE, Pluronic F127, and PSMA.

A typical encapsulation matrix, 1,2-distearoyl-*sn*-glycero-3-phosphoethanolamine-*N*-(polyethylene glycol) (DSPE-PEG₂₀₀₀) and DSPE-PEG₅₀₀₀-folate, was widely used to prepare fluorescent nanoparticles with AIE fluorogens due to the good biocompatibility. Liu and co-workers developed A1 FNPs by

using DSPE-PEG₂₀₀₀ and DSPE-PEG₅₀₀₀-folate as shown in Scheme 1.⁵⁰ A1 is a typical AIE fluorogen, which showed very weak fluorescence in THF solution but high fluorescence in water after nano-aggregates formation. FNPs with the modification of folic acid groups can be prepared through one-step formation of hydrophobic AIE fluorogens-doped nanoparticles by encapsulating A1 in a mixture of DSPE-PEG₂₀₀₀ and DSPE-PEG₅₀₀₀-folate. The folate density can be adjusted by varying the feed ratio of DSPE-PEG-folate to DSPE-PEG for fluorescent nanoparticle preparation. The nanoparticles showed good selectivity between MCF-7 and NIH/3T3 cells due to the specific folate receptor-mediated endocytosis for MCF-7 cells and the presence of long PEG chains which suppressed nonspecific cellular uptake of the nanoparticles. Later, Liu and co-workers reported the fabrication of DSPE-PEG encapsulated A2 FNPs (Fig.1) with an emission peak-wavelength located at 577 nm, which were utilized as efficient optical probes for *in vivo* sentinel lymph node mapping of mice.⁵¹ From Fig.1, the mixture solution of A2 and mPEG-DSPE was evaporated and dried under vacuum in a rotary evaporator. After adding deionized water into the obtained lipidic film and then sonicating for 2 min, an optically clear suspension containing A2@PEG can be obtained. The as-prepared FNPs exhibited ultra-small size, high monodispersity, excellent chemical stability and aggregation-enhanced emission (AEE). When DSPE-PEG-maleimide was used as the matrix, thiol-RGD (arginine-glycine-aspartic acid) was realized to endow NPs with tumor cell marking ability. The RGD-functionalized A2 FNPs were also applied for targeted xenografted tumor imaging in mice.

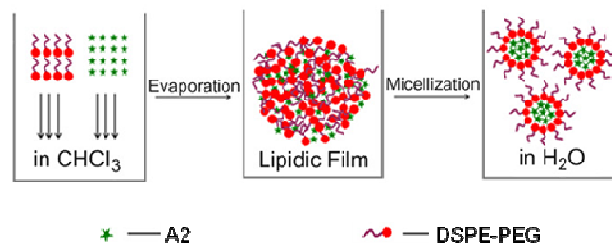
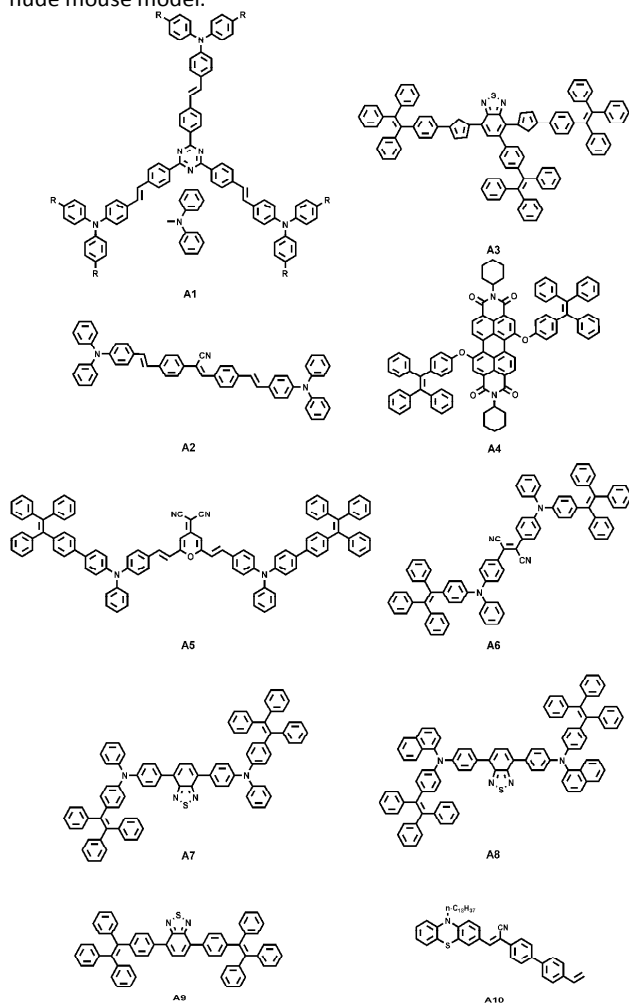


Figure 1. A schematic illustration for the preparation of A2@PEG nanomicelles. (Reproduced from Ref. 51 with permission from Copyright 2011 Elsevier B.V.).

A red emissive fluorogen A3 with AIE-activity has been reported. The A3-loaded FNPs encapsulated with DSPE-PEG₂₀₀₀ were formed spontaneously upon sonication.⁵² The average size of A3 FNPs was about 63 nm and the fluorescence quantum yield was 14%. The A3 FNPs can be internalized in MCF-7 cells without causing adverse event. To further avoid the interference of background, Tang and co-workers reported a Red-NIR emissive AIE fluorogen A4.⁵³ A4 was obtained by conjugating TPE with 3,4,9,10-tetracarboxylic perylene bisimide (PBI). Encapsulation of A4 with a mixture of DSPE-PEG₂₀₀₀ and DSPE-PEG₅₀₀₀-Folate yielded A4 FNPs with Red-NIR emissive. The A4 FNPs have uniform average size of 76 nm in water. Studies on the staining of MCF-7 breast cancer cells and *in vivo* imaging of a tumor bearing mouse model with the A4 NPs reveal that they can served as effective fluorescent probes

for cancer cell and in vivo tumor diagnosis. In addition, Tang and coworkers have reported another FR/NIR emissive AIE fluorogen A5.⁵⁴ The A5 FNPs was about 53 nm with bright FR/NIR fluorescence, which the emission maximum appeared at 684 nm with an intense emission tail extended to over 80 nm and the fluorescence quantum yield of A5 FNPs can reach to 13%. Moreover, the high two photon absorption cross section and FR/NIR emission of A5 NPs allow two-photon fluorescence imaging of MCF-7 breast cancer cells and ensure the efficient penetration depth in tumor tissue (about 400 μm) upon intratumoral injection on a C6 glioma tumor-bearing nude mouse model.



Scheme 2. Chemical structures of A1-A10

Due to the abundant vibration energy levels of the twisted conformation for AIE fluorogens, as well as the large conformational difference between the ground state and the first singlet excited state, the AIE FNPs generally have broad emission spectra, which limited their application in multiplexing. Liu and coworker have reported a Förster resonance energy transfer (FRET) strategy to achieve a narrow NIR emission FNPs through co-encapsulated A6 and NIR775 in DSPE-PEG (as shown in Fig. 2).⁵⁵ The AIE fluorogen A6 has been

widely investigated and first reported by Tang and coworkers.⁵⁶ There are good spectral overlap between the emission of A6 and the absorption of NIR775, which leads to efficient energy transfer. In this work, with increasing NIR mass ratios from 0.5% to 1.5%, the emission from 550 to 750 nm was quenched a lot, while the emission from 750 to 900 nm, which originated from NIR775, increased gradually. Further increasing the NIR775 concentration resulted in reduced NIR emission intensity caused by the ACQ phenomenon of NIR775. When the mass ratio of NIR775 was 1.5%, the emission intensity of NIR775 upon excitation at 510 nm was 47-fold higher than that upon direct excitation of NIR775 at 760 nm. The obtained FNPs showed sharp NIR emission with a band width of 20 nm, a large Stokes shift of 275 nm and a fluorescence quantum yield of 7%. In vivo imaging studies revealed that the A6/NIR775 FNPs were more efficient upon FRET channel than direct excitation at 704 nm (Fig. 2a & b). The FRET strategy overcomes the intrinsic limitation of broad emission spectra for AIE FNPs, which opens new opportunities to synthesize organic FNPs with high brightness and narrow emission for potential applications in multiplex sensing and imaging.

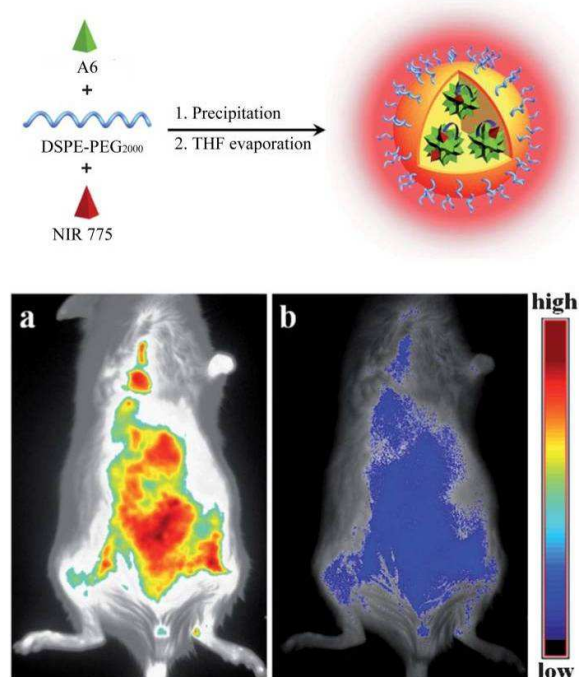


Figure 2. Schematic illustration of the fabrication of A6 and NIR775 co-loaded NPs. In vivo fluorescence imaging of mice after intravenous injection of TPETPAFN-1.5% NIR775 NPs upon excitation at (a) 523 nm and (b) 704 nm, respectively. (Reproduced from Ref. 55 with permission from Copyright 2014 The Royal Society of Chemistry).

A mixture of DSPE-PEG and DSPE-PEG-NH₂ was chosen as the encapsulation matrix to endow the AIE FNPs with biocompatibility and surface functionality.⁶¹ The yielded A6-based NPs with uniform size of 30 nm in water, near-infrared emission and fluorescence quantum yield of 24%. Cell penetrating peptide derived from HIV-1 transactivator of

transcription (Tat) protein was further functionalized to the dots, and the single nanoparticle imaging reveal that the Tat-A6 dots are 10-fold brighter than the commercial Qtrackers 655. It was found that the Tat-AIE dots could trace MCF-7 cells for 10-12 generations in vitro and C6 cells for 21 days in vivo. One and two photon excited ex vivo tumor images were taken to highlight the deep tissue imaging ability of the Tat-AIE dots. This is the first successful demonstration of the AIE dots for in vitro and in vivo long-term cell tracing. Similar Tat-AIE dots, which have been reported by Tang's and Liu's group, were prepared by using A7, A8 and A9.⁵⁷⁻⁵⁸ It is noteworthy that the A7, A8 and A9 AIE dots have fluorescence quantum yields as high as 55%, 67% and 64% in water, respectively, ensuring high contrast in cell imaging. These Tat-AIE dots have displayed good performance in long-term non-invasive in vitro cell tracing and superior performance compared to their counterparts of inorganic quantum dots and green fluorescent protein (GFP). It should be noted that these FNPs have been termed AIE dots due to their small and uniform sizes and outstanding performance, which may open a new area in the development of fluorescent probes for monitoring biological processes.

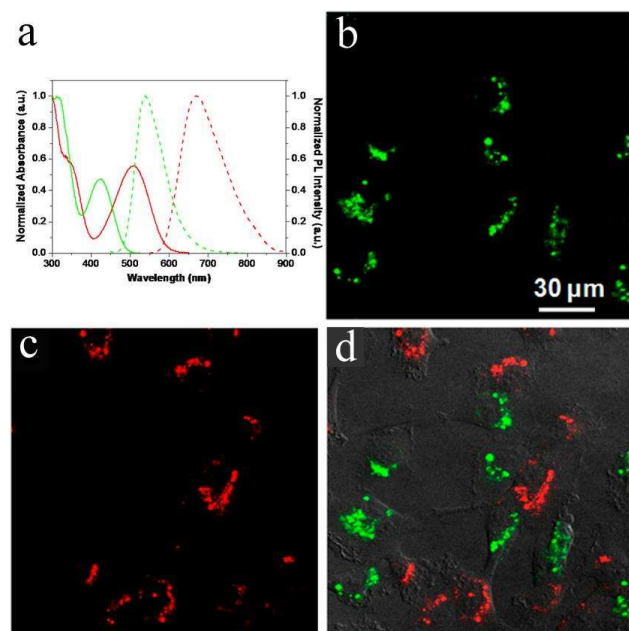


Figure 3. a) UV-vis absorption (solid) and PL (dashed) spectra of GT-AIE (green) and RT-AIE (red) dots in water; b)-d) Simultaneous monitoring of HT1080 fibrosarcoma cells labeled with 2 nM of either A6 dots or A9 dots after coculture for 12 h. Images are recorded under excitation at 458 nm with b) 480–560 and c) 670–800 nm bandpass filters. d) Fluorescence/transmission overlay image. (Reproduced from Ref. 59 with permission from Copyright 2013 American Chemical Society).

NIR fluorogen A6 and green fluorescent fluorogen A9 were further used to simultaneously discriminate different populations of cancer cells both in culture medium and animal organs.⁵⁹ A6 and A9 dots were prepared by nanoprecipitation by using DSPE-PEG-maleimide as matrix, and functionalized with thiol-decorated Tat peptide. Due to their distinct emission

peaks at 539 and 670 nm with minimal spectral overlap (Fig. 3a), Tat modified A6 and A9 dots were used to label the interaction between two groups of highly motile HT1080 cells (Fig. 3b-d). The imaging of the lung tissue section collected from the mouse injected with the mixture of C6 cells labeled by these two dots revealed no fluorescence signal interference. By using A6 as NIR fluorogen and diethylenetriaminepentaacetic (DTPA)-gadolinium(III) as magnetic resonance reagent, dual-modality AIE dots with both fluorescent and magnetic properties were further prepared.⁶⁰ The obtained fluorescent-magnetic AIE dots have both high fluorescence quantum yield (25%) and T1 relaxivity ($7.91 \text{ mM}^{-1} \text{ s}^{-1}$) in aqueous suspension. The modification of Tat peptide allowed these AIE dots to accurately analyze the biodistribution of labeled cells through gadolinium(III) ion quantification. The excellent performance of these AIE dots makes it possible to monitor cell interaction and migration during metastasis using a mouse model.

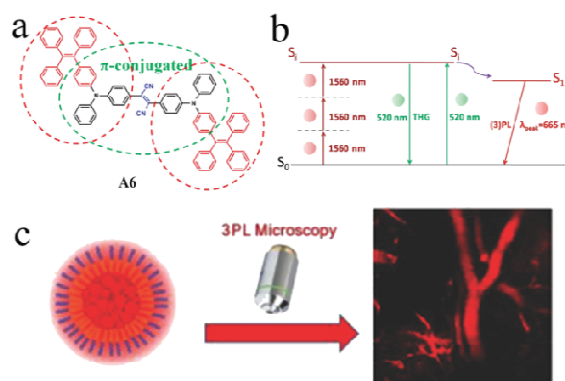


Figure 4. a) Molecular structure of A6, (b) Diagrams showing the proposed excitation mechanisms of THG and THG-induced 1PL and (c) scheme for 3PL microscopic imaging of brain blood vessels of a mouse (intravenously injected with A6-dots). (Reproduced from Ref. 61 with permission from Copyright 2015 Wiley-VCH).

AIE dots were also applied for two-photon fluorescence imaging of intravital blood vessels.⁶¹⁻⁶⁴ For the large multiphoton absorption cross-section and other non-linear optical (NLO) effects, as well as the far red/NIR emission upon excitation, A6 based nanoparticles have been applied in deep, real-time, and long-time NLO microscopic in vivo imaging by He and co-workers⁶¹. They observed simultaneous 3PL/4PL, THG, and FHG of A6 in the solid state. Moreover, aggregation-induced THG enhancement and aggregation-induced 3PL were also found (Fig. 4b). A6-doped-nanoparticles were further used for multimodal NLO microscopic imaging of tumor cells, as well as 3PL in vivo imaging of mouse brains (Fig. 4c). Liu and co-workers⁶² prepared A9 dots with a uniform size of 33nm, a high quantum yield of 62% and a large two-photon absorption action cross section ($6.3 \times 10^4 \text{ GM}$ at 810 nm). From the wide-field fluorescence images of single particles, the AIE dots are brighter than QD655. Real-time two-photon blood vasculature imaging in live mice with AIE dots is investigated in three intravital two-photon fluorescence imaging models, the brain, bone marrow, and skin. The major blood vessels, the smaller capillaries in the pia mater and microvasculature in the brain

could be visualized with the AIE dots. The imaging depth was up to 424 μm and resolution was very high (few micrometers). The vascular systems in skull bone marrow and skin were also imaged to demonstrate the *in vivo* two photon fluorescence imaging ability of AIE dots. Similar results have been reported for A6 dots and A11 dots.^{63,64} These AIE dots possess good photostability, ultra bright, large cross-section values, which provide a novel platform to visualize blood vessels *in vivo* for better understanding of biological processes, such as angiogenesis and vascular leakage.

Liu and co-workers further demonstrated the application of Tat-A6 dots for long-term tracking of bone marrow stromal cells (BMSCs) with mesenchymal properties by using an ischemic stroke model.⁶⁵ These dots contained good long-term cell tracing property. After 18 days of continuous subculture, 51.0% of the Tat-M6 dots-treated cells remained efficiently labeled. Upon transfusion in an ET-1 stroke model, *ex vivo* analysis revealed that the Tat-A6 dots treated BMSCs cells could preferentially accumulate in the injured tissue but not the intact ones (Fig. 5 b-c). This result helps us to understand the behaviour and function of BMSCs in ischemic strokes. Furthermore, the Tat-A6 dots could also afford dual-modality imaging probes which are desired for real-time *in vivo* monitoring of the migration and function of BMSCs in brain tissues (Fig. 5a).

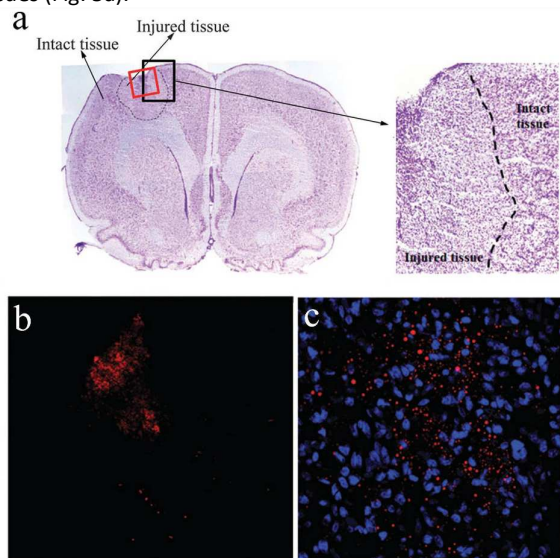


Figure 5. a) Thionin staining of brain tissue collected from rats with ET-1 induced ischemic stroke after 7 days upon BMSC transfusion. (b) Fluorescence images of the lesion site in sectioned brain tissue collected from rats at day 7 post transfusion of Tat-A6 dots-labelled BMSCs. (c) Fluorescence images of the lesion site under a high magnification. (Reproduced from Ref. 65 with permission from Copyright 2014 Royal Society of Chemistry)

Due to the excellent photostability, ultra brightness and long term cell tracking property of Tat-A6 dots, Liu and co-workers explored their applications in noninvasive long-term tracking of adipose-derived stem cells (ADSCs) and monitored their regenerative capability in an ischemic hind limb model.⁶⁶ The *in vitro* ADSC tracing experiments demonstrate that the Tat-A6

dots possess superior retention in ADSCs than commercially available cell trackers, Qtracker 655 and PKH26. The ADSCs tracking studies from ischemic hind limbs of mice show that the Tat-A6 dots can precisely track ADSCs and report the regenerative capacity of ADSCs *in vivo* for 6 weeks (Fig. 6b-d). It is worth noting that 6 weeks observation is the longest *in vivo* cell tracking duration among the currently available exogenous fluorescent cell trackers (Fig. 6a).

2.2 Other polymer encapsulated nanoparticles

Jen and co-workers demonstrated a FRET strategy, and showed that the different encapsulation matrices could affect the quantum yields of nanoparticles.⁶⁷ In this work, three block copolymers poly-(ϵ -caprolactone)-*b*-poly(ethylene glycol) (PCL-PEG), PS-PEG, and poly(styrene)-*b*-poly(methacrylic acid) (PS-PMAA), were applied to encapsulate two AIE fluorogens, A11 and A12. Among the nanoparticles based on these three co-polymers, PS-PMAA FNPs presented highest quantum yields of 22.3% for A11 and 62.1% for A12. The longer lifetimes for PS-PMAA NPs suggest that the PS core is more efficient in promoting radiative decay of AIE fluorogens. Then A11 and A12 were co-encapsulated into a single nanoparticle served A11 as the energy donor and A12 as the energy acceptor. Upon incubation with RAW cells by using the A11/A12 co-encapsulated nanoparticles, the green fluorescence is greatly suppressed while intense red fluorescence is observed.

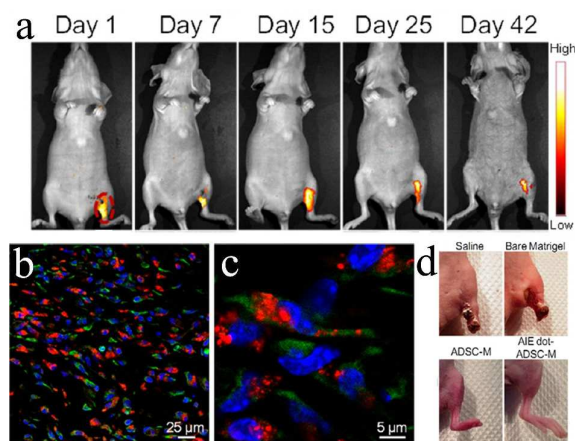
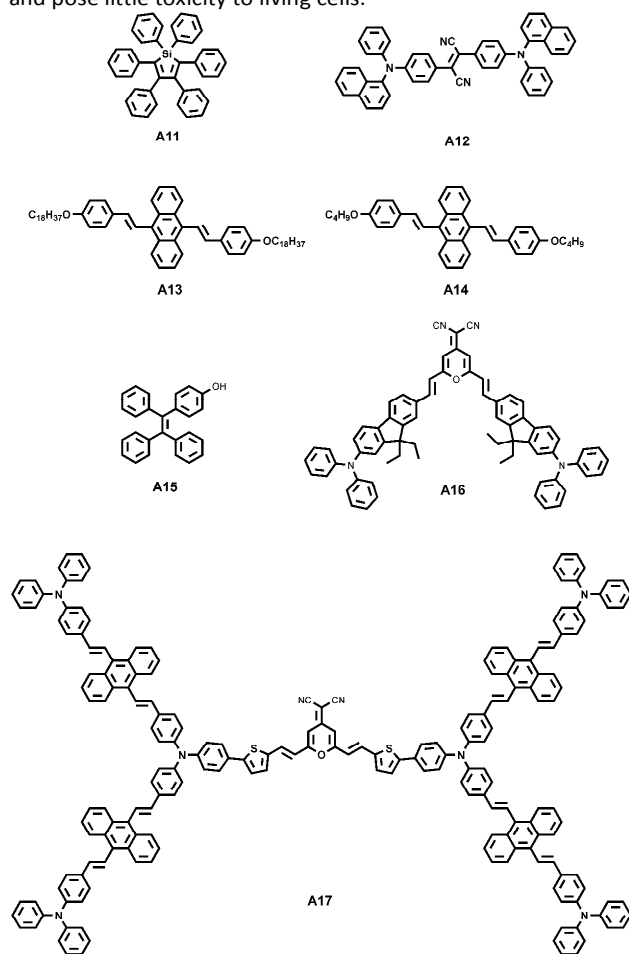


Figure 6. a) Representative time-dependent *in vivo* fluorescence images of the ischemic hind limb-bearing mouse that was intramuscularly injected with AIE dot-labeled ADSC-containing Matrigel; Tracking of ADSCs *in vivo* at single-cell resolution: a) representative CLSM image of ischemic hind limb slices from mice after administration of AIE dot-labeled ADSC-containing Matrigels for 30 days; c) enlarged CLSM image in b; d) the representative photographs of the ischemic hind limb-bearing mice after 30 days post treatment. (Reproduced from Ref. 66 with permission from Copyright 2014 American Chemical Society).

Wei and co-workers prepared AIE-based fluorescent nanoparticles via mixing of AIE units A13 and a commercial surfactant F127.⁶⁸ The A13-F127 FNPs exhibit good water solubility and biocompatibility. The cell imaging application revealed that A13-F127 NPs could easily be observed in cells. Our group recently reported a new AIE FNPs by incorporation of the hydrophobic AIE fluorophore A14 and A12, using Pluronic

F127-folic acid adduct (F127-FA) as the encapsulation matrix.⁶⁹ Due to the spectrum overlap between A14 and A12, the co-encapsulated nanoparticles have a 3.0-fold amplified A12 emission signal via FRET mechanism. These FNPs were further used for targeted folate receptor overexpressed MCF-7 breast cells and revealed that these nanoparticles could specific targeting effect for FR-overexpressed cancer cells.

A novel near-infrared AIE molecule A17 by coating a disc-like red emission fluorophore with a propeller-shaped AIE fluorophore has been reported by our group.⁷⁰ By using A17 as the core and biocompatible polymer PS-PVP as the encapsulation matrix, the A17-PS-PVP dots were prepared and the intensive red emission with the fluorescence quantum yield of 12.9% was observed. In vitro cells experiment revealed that the mono-dispersed A17-PS-PVP dots can stain both the cytoplasm and the nuclei with a strong red fluorescence signal, and pose little toxicity to living cells.



Scheme 3. Chemical structures of A11-A17.

Apart from the amphiphilic polymer, Tang and co-workers reported bovine serum albumin (BSA) FNPs with high brightness and low cytotoxicity by using the A5 as AIE fluorogen and BSA as polymer matrix.⁷¹ The BSA FNPs can be applied for in vitro and in vivo bioimaging, which are successfully demonstrated by using MCF-7 breast-cancer cells

and a murine hepatoma-22 (H22)-tumor-bearing mouse model, respectively. Because of the enhanced permeability and retention effect, the BSA FNPs also show prominent tumor-targeting ability. In addition, Liu and co-workers reported a far-red/near-infrared (FR/NIR) FNPs by co-encapsulation of conjugated polymer donor, poly[9,9-bis(2-(2-(2-methoxyethoxy) ethoxy) ethyl) fluorenyldivinylene] (PFV) and a fluorogen acceptor A5 using BSA as the encapsulation matrix.⁷² This BSA FNPs result in a 5.3-fold amplified emission signal via fluorescence resonance energy transfer. The BSA matrix allows further functionalization with RGD peptide for specific recognition of integrin receptor-overexpressed cancer cells. These results clearly indicate that FRET is an efficient strategy to further increase the luminescence of AIE-based fluorescent nanoparticles.

Our group reported a novel Near-infrared emissive organic dots by using polymer poly(styrene-co-maleic anhydride) (PSMA) as the co-encapsulation matrix and novel fluorogen A18 as the emissive core.⁷³ These dots have small particle size of about 20 nm, a large Stokes shift of 304 nm and really high fluorescence quantum efficiency of 20%. By esterification reaction, streptavidin were bio-conjugated to the surface of these dots. SA-dots possess very good biocompatibility and almost no toxicity for cells. In vitro cells experiment revealed that there are no detectable nonspecific binding and the SA-dots can specifically and effectively label the MCF-7 cell surface (Fig. 7).

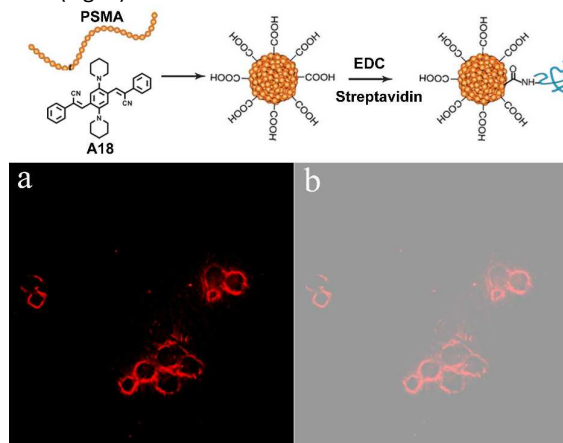


Figure 7. a) Fluorescence imaging and b) overlay images of cell surface marker (EpCAM) in MCF-7 cells labeled with SA-dot. (Reproduced from Ref. 73 with permission from Copyright 2015 Royal Society of Chemistry).

3 Covalent AIE copolymer nanoparticles

Despite many impressive advances in the fabrication of non-covalent FNPs by using physical encapsulation, various covalent strategies have been introduced into the fabrication of FNPs based on AIE fluorogens. At the same time, the strategies of versatile preparation, such as modified reactive groups to integrate drugs and targeting agents for multifunctional biomedical applications, have also been developed.

3.1 Covalently binding AIE fluorogens to amphiphilic block copolymer

A number of chemical reactions have been utilized to fix the fluorophoric units to the amphiphilic copolymer or the biopolymer, typical examples of which include isothiocyanate-(ITC) and amine-mediated reactions, Schiff base reactions, alkoxyl and acyl group based reactions.

For the high reaction efficiency and rate of ITC- and amine-mediated reactions, Tang and co-workers^{29, 74} reported the fabrication of highly fluorescent TPE-chitosan (TPE-CS) bioconjugates through the attachment of a large number of AIE fluorogens to a CS chain. TPE is an archetypical AIE fluorogen, which possess a unique solid state emission property. TPE was firstly functionalized with a reactive ITC group. Then, the obtained TPE-ITC intermediate was used to label CS. The fluorescence output of TPE-CS bioconjugate can be enhanced to a great extent by simply increasing its degree of labeling. The internalized TPE-CS bioconjugate microparticles did not leak out in the coculture system, allowing visual differentiation of one specific cell line from the other unstained cell lines. The outstanding intracellular retention of the TPE-CS bioconjugate microparticles would permit the stained cells to be traced for as long as 15 passages. This makes the TPE-CS bioconjugates promising candidate materials for applications in biomedical areas as long-term cellular tracers which were under high demand in such important areas as cancer metastasis, neuron networking, embryo development, and stem cell differentiation.

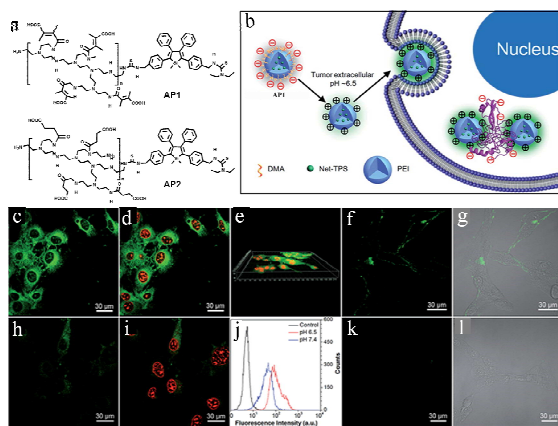


Figure 8 a) Chemical structures of AP1 and AP2. b) Schematic illustration of AP1 as a pH-responsive light-up nanoparticle probe for targeted cancer cell imaging. Confocal laser scanning microscopy (CLSM) images of the MCF-7 cancer cells incubated with AP1 (green fluorescence) at (c and d) pH 6.5 and (e and f) pH 7.4 for 1 h at 37°C, respectively. The cell nuclei were stained by PI (red fluorescence) for (d) and (f). (g) 3D confocal image of MCF-7 cancer cells incubated with AP1 at pH 6.5. (h) Flow cytometry histograms of pure MCF-7 cancer cells and the cells incubated with Net-TPS-PEI-DMA at pH 6.5 and 7.4. CLSM fluorescence and fluorescence/transmission overlay images of MCF-7 cancer cells treated with AP1 at (f and g) pH 6.5 and (k and l) 7.4 at 4°C. (Reproduced from Ref. 75 with permission from Copyright 2014 The Royal Society of Chemistry).

In tumor microenvironments, pH-responsiveness is of particular interest and it has been extensively investigated in controlled drug delivery for better cancer targeting and

treatments. A pH-responsive light-up nanoparticle probe with AIE features was designed and synthesized by Liu's group⁷⁵. The probe carries negative charges and shows very weak fluorescence under physiological conditions. Under acidic conditions (pH=6.5), the surface charges of AP1 switch to positive, which endow the nanoparticle probe with the abilities to be internalized into the cancer cells as well as significantly turn on its fluorescence (Fig. 8b). The in vitro and in vivo experiments demonstrate that AP1 can significantly light up the cancer cells, which is able to serve as an efficient pH-responsive light-up nanoparticle probe for targeted cancer cell imaging and in vivo tumor imaging. Intense green fluorescence is observed inside the MCF-7 cancer cells at pH 6.5 (Fig. 8c-d), while much weaker fluorescence is observed at pH 7.4 (Fig 8 h-i). Additionally, the flow cytometry data indicate that the average fluorescence intensity of each cell incubated with AP1 at pH 6.5 is 3.0-fold higher as compared to that at pH 7.4 (Fig. 8j). The cytotoxicity results also reveal that AP1 shows low cytotoxicity to normal cells and relatively high cytotoxicity to cancer cells. The high cytotoxicity against cancer cells also possess the suppression of Akt pathway and the activation of apoptotic pathway.

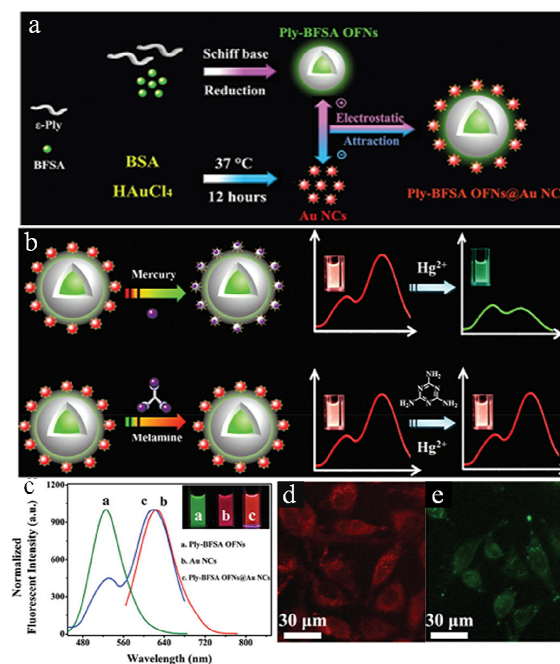


Figure 9 a) Schematic illustration of the synthesis of Ply-BFSA@ Au NCs; b) Schematic illustration of the dual-emission Ply-BFSA OFNs @ Au NCs as a ratiometric fluorescence probe for the detection of mercury and melamine. c) fluorescence emission spectra of (a) Ply-BFSA OFNs (green line), (b) Au NCs (red line), and (c) Ply-BFSA OFNs @Au NCs (blue line). The inset photo shows the corresponding fluorescence colors under UV illumination. Fluorescence images of HeLa cells after incubation with Ply-BFSA OFNs @Au NCs for 4 h, d) without Hg²⁺, e) with Hg²⁺ (400 nM) for 1 h. (Reproduced from Ref. 77 with permission from Copyright 2015 The Royal Society of Chemistry).

Different from the ITC reaction, Wei and co-workers⁷⁶ provided a facile strategy for the preparation of water soluble FNPs from a stable C-N bond-linked TPE-CS polymer, which

were prepared through the formation of a Schiff base *via* condensation between hydrophobic 4-(tetraphenylethene)benzaldehyde and primary amine groups-containing hydrophilic 3-polylysine, and then reduced by NaBH₄ to afford stable products with the C-N covalent bond. The obtained TPE-CS showed amphiphilic properties and apparent AIE features, which could form intense fluorescent emission FNPs in an aqueous environment. These FNPs with strong fluorescence and high biocompatibility were benefited for cell imaging applications.

Recently, Ouyang and co-workers⁷⁷ reported a dual-emission ratiometric fluorescence probe based on the ϵ -polylysine labeled AIE FNPs and BSA stabilized Au nanoclusters, which are linked by electrostatic attraction (Fig. 9a). Since the modification of ϵ -polylysine and BSA, the prepared dual-emission ratiometric FNPs have good biocompatibility, which gives the probe potential applications in biological imaging and detection. Due to the strong affinity metallophilic Hg²⁺-Au interaction and stronger affinity Hg²⁺-N interaction, the fluorescence of the Au NCs is quenched by Hg²⁺ and recovered by melamine, while the fluorescence of the AIE-OFNs remains constant owing to the protection of Polylysine (Fig. 9b). The probe can be used for not only visual but quantitative determination of Hg²⁺ as well as melamine. As shown in Fig. 9d, in the absence of Hg²⁺, the cells colored by the Ply-BFSA OFNs@Au NCs can be clearly observed; when 400 nM Hg²⁺ was introduced to the HeLa cells for 1 h, the cell color changed to green (Fig. 9e). The results indicated that the dual-emission nanoprobe could be used for the ratiometric fluorescence detection imaging of Hg²⁺ in living HeLa cells. This dual emission hybrid nanoparticles broadens the application of AIE-based FNPs, and supplies a new way to prepare more sensitive, biocompatible, and visual ratiometric fluorescent probes.

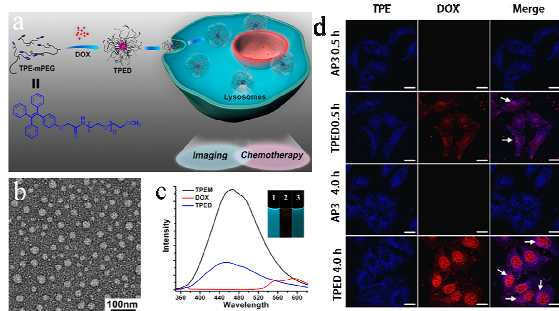


Figure 10 a) Schematic illustration of DOX-loaded self-assembly micelle (TPED) with aggregation-induced emission (AIE) as a novel multifunctional theranostic platform for intracellular imaging and cancer treatment. b) TEM image of AP3 after staining with 1% uranyl acetate. c) Fluorescence spectra of AP3, free DOX, and TPED excited at 330 nm. (inset) Photograph showing fluorescence of AP3 (1), DOX (2), and TPED (3) under UV light (365 nm). d) Spatial distributions of TPED and TPED in MCF-7 cells. CLSM images of the distribution of self-indicating AP3 and TPED. MCF-7 breast cancer cells were incubated with AP3 (75 μ M) and TPED (AP3 75 μ M and DOX 5.0 μ M) for 0.5 and 4 h. Scale bars are 20 μ m. (Reproduced from Ref. 79 with permission from Copyright 2014 American Chemical Society).

Alkoxy and acyl groups are the common way to fix fluorophoric units to the polymers. Wei and co-workers⁷⁸

developed a novel one-pot strategy for the fabrication of AIE-based FNPs via a combination of RAFT polymerization and enzymatic transesterification. During this procedure, a hydrophobic tetraphenylethene-functionalized AIE dye A15 with a hydroxyl end functional group and a hydrophilic polyethylene glycol monomethyl ether (mPEG-OH) were simultaneously attached onto the methacrylate monomer via enzymatic transesterification. The Mn of the obtained polymers was about 4700 g/mol with a narrow PDI (\sim 1.30), and the molar fractions of TPE and PEG in the polymer was about 30.5% and 69.5%, respectively. The amphiphilic copolymer formed after RAFT polymerization of the functionalized methacrylate monomers tended to self-assemble into FNPs with the hydrophobic AIE core covered by a hydrophilic PEG shell. Such FNPs also showed excellent fluorescence in aqueous solution owing to the introduction of the AIE component.

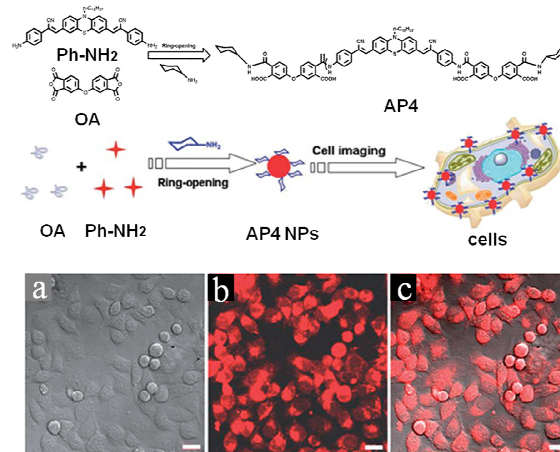


Figure 11 Schematic showing the preparation of glycosylated AP4 NPs through ring-opening polymerization (ROP) and cell imaging applications of AP4 NPs. CLSM images of A549 cells when they were incubated with 10mg/mL AP4 NPs for 3 h. (A) Bright field, (B) excited with 543 nm laser, (C) merge image of A and B. (Reproduced from Ref. 80 with permission from Copyright 2014 The Royal Society of Chemistry).

Similarly, Liang and co-workers⁷⁹ reported a drug delivery system (DDS) using TPE to fabricate a self-assembly micelle with AIE feature. Both AP3 and TPED were spherical in shape, with a diameter of about 30 nm (Fig 10b), and had good dispersion. High of FNPs makes the nanocarriers visible for high-quality imaging, and the switching on and off of the AIE properties is intrinsically controlled by the assembly and disassembly of the FNPs. (Fig. 10c) This DDS was tested for doxorubicin (DOX) delivery and intracellular imaging. For the DOX-loaded FNPs, the DOX content reached as much as 15.3% by weight, and the anticancer efficiency was higher than for free DOX. Meanwhile, high-quality imaging was obtained to trace the intracellular delivery of the FNPs. After incubating cancer cells with TPED for 4 h, the red fluorescence of DOX was mostly visible in the nucleus, which indicated that nanocapsules could release DOX into the nucleus. In addition, as the incubation time increased from 0.5 to 4 h, the

fluorescence intensity of DOX and TPE both increased, indicating the increased cellular uptake of AP3 and TPED.

The glycosylated AIE dyes based FNPs were facilely prepared through one-pot ring-opening reaction by Wei's group⁸⁰. This kind of reaction can be occurred under room temperature and air atmosphere without needing catalysts and initiators, which is rather simple, effective and scalable (Fig. 11a). On the other hand, due to the existence of hydrophilic Glu and carboxyl groups on the surface of AP4 FNPs, thus obtained AIE-based copolymer are readily self assembled into FNPs in pure aqueous solution. These FNPs possess numerous excellent properties such as uniform morphology, high water dispersibility, strong red fluorescence and excellent biocompatibility, making them highly potential for various biomedical applications. More importantly, due to the advantages of glycosylated polymers, AP4 FNPs are expected exhibited different properties for biomedical applications. As shown in Fig. 11a-c, the cell uptake of AP4 FNPs was clearly observed after cells were incubated with AP4 FNPs for 3 h. The successful dyeing of cells with fluorescent organic nanoparticles implies the potential biological imaging applications of AP4 FNPs.

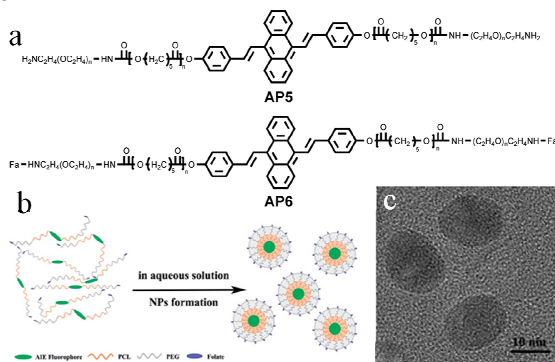


Figure 12 Chemical structures of AP5 and AP6, b) Schematic drawing of the preparation of AIE Pdots. c) Enlarged TEM image of AP6 Pdots. (Reproduced from Ref. 81 with permission from Copyright 2014 The Royal Society of Chemistry).

Fluorescent block amphiphilic copolymers are one of the most important bioimaging materials which are highly desirable for early stage cancer diagnosis and treatment. Our group reported a series of conjugated amphiphilic copolymer⁸¹ which contains an AIE fluorophore, 9,10-bis(4-hydroxystyryl) anthracene, hydrophobic poly(3-capro-lactone) segments, hydrophilic poly(ethylene glycol) segments and folate groups (Fig. 12a). These amphiphilic copolymer can easily form the monodisperse polymer dots (Pdots) through a self-assembly process. The self-assembled AIE Pdots are stable in aqueous solution with an average diameter of 15 nm (Fig. 12c). These AIE Pdots have high fluorescence quantum efficiency of 27.0%. Furthermore, the folic acid functionalized AP6 dots show targeting ability to HeLa cells which overexpress the folate receptor compared with normal 3T3-L1 cells. These AIE Pdots also show good stability and little toxicity to living cells and thus can provide a strategy to construct bright and highly photobleaching resistant fluorescent probes for bioimaging.

3.2 Polystyrene block copolymer nanoparticles

Except covalently bounding organic dyes to amphiphilic polymers, polymerization is an important method which has been previously used for fabrication of FNPs via controllable incorporation of polymerizable organic dyes into polymers. The general driving force for the formation of these FNPs can be ascribed to the self-assembly of these amphiphilic copolymers in aqueous solution. During the self-assembly procedure, hydrophobic segments including organic dyes are encapsulated in the core, while the hydrophilic segments are covered on the hydrophobic core as the shell, which can be extended into water with high water dispersibility. Hence, a series of covalent fabrication methodologies of AIE-based FNPs have been reported and developed, including emulsion polymerization, reversible addition fragmentation chain transfer (RAFT) polymerization, anhydride ring-opening polymerization and cross-linked polymerization.

Through the emulsion polymerization, Wei's group reported a novel strategy for fabrication of AIE-based FNPs.⁸² During polymerization procedure, a polymerizable AIE fluorogen (Z)-3-(10-octadecyl-10H-phenothiazin-3-yl)-2-(4'-vinyl-[1,1'-biphenyl]-4-yl)acrylonitrile (A10) with a double bond end functional group as one of components was facilely incorporated with acrylic acid (AA) and styrene (St) into the copolymer. Due to the hydrophobic nature, A10 tends to aggregate in the core of FNPs with other hydrophobic St units. However, the hydrophilic AA components were covered on the hydrophobic core and served as the hydrophilic shell. Thus the obtained FNPs (A10-Pst) emitted strong fluorescence and high water dispersibility owing to the AIE features of A10 and the surface covered with hydrophilic layers. These FNPs showed spherical morphology, uniform size and excellent biocompatibility, making them promising for cell imaging applications.

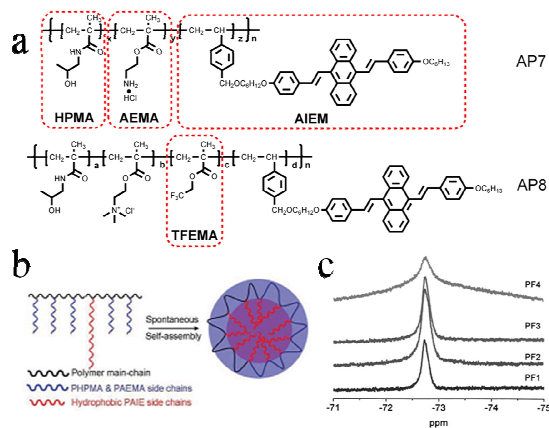


Figure 13 a) Chemical structures of AIE fluorophore-containing amphiphilic copolymers. b) A possible schematic drawing of the micelles formed from the polymers using a flower-micelle model. c) ¹⁹F NMR spectra of PF1 to PF4 in H₂O and DMSO (98 : 2 by volume) at 10 mg/m (Reproduced from Ref. 83&84 with permission from Copyright 2012 The Royal Society of Chemistry).

RAFT polymerization is distinguished from all other methods of controlled/living free-radical polymerization with a wide range of monomers and reaction conditions and in each case it

provides controlled molecular weight polymers with very narrow polydispersities. Our group developed several series of PHPMA based random copolymers with hydrophobic AIE fluorophores^{83, 84}. We first reported the development and bioapplications of a new series of AIE-fluorophore-containing random copolymers AP7, which polymerized from an AIE fluorophore with a styrene moiety as a monomer (AIEM), N-(2-hydroxypropyl)methacrylamide (PHPMA), and 2-aminoethyl methacrylate (AEMA) (Fig 13a). Through controlling the molar ratio of each component, we can get a serious amphiphilic copolymer. Results show that the AIE fluorophores aggregate in the cores of the FNPs formed from the amphiphilic random copolymers and polymers with more hydrophobic AIE fluorophores facilitate stronger aggregations of the AIE segments to obtain higher quantum efficiencies, up to 13%. These FNPs with biocompatible polymers such as the PHPMA enables its application in biological condition for bioimaging and endows the noncytotoxicity to cells. However, in order to improve fluorescence quantum yields of these FNPs, we further introduced a hydrophobic component, 2,2,2-trifluoroethyl methacrylate (TFEMA), into the copolymer AP8. It makes AIEM aggregate closely to achieve higher fluorescence quantum yields. Using 1 mol% of AIE fluorophores with the tuning of the molar fraction of TFEMA, the fluorescence quantum yield of FNPs can reach to 40%. Compared with the quantum yield of AP7 FNPs, the fluorescence quantum yield of AP8 FNPs is almost 4 fold enhancement, which indicates the importance of the fluorine segments for getting high quantum yields of these AIE-based FNPs. All the FNPs are cell permeable and located in the cellular cytoplasm area. Cellular uptake was demonstrated to be through the endocytosis mechanism, which is time and energy dependent. According to the introduction of ¹⁹F segments, we investigated the spin-lattice relaxation time (T1) and spin-spin relaxation time (T2) of these copolymers (Fig. 13c). The polymers showed reasonable T1 and T2 values, especially influence on T2. These multifunctional FNPs may broaden the application of AIE-based FNPs not only for fluorescence imaging but also for ¹⁹F magnetic resonance imaging.

Xu and co-workers⁸⁵ reported a series of new homopolymers with various degrees of polymerization, i.e., poly[(2-(4-vinylphenyl) ethene-1,1,2-triyl) tribenzene] homopolymers, which were also successfully synthesized by RAFT polymerization. The homopolymers exhibited a significant AIE effect with 100-fold enhancement of emission intensity from solution to nanosuspension. The homopolymers can assemble themselves to AIE-based FNPs by quickly charging THF solution into deionized water. The FNPs exhibited strong blue fluorescence, good dispersibility, stability and biocompatibility, which can internalize to HeLa cells, specifically the cytoplasm. The current study provides a new framework to fabricate more stable surfactant-free AIE FNPs and shows great potential biomedical applications.

Similarly, Wei and co-workers⁸⁶ presented the fabrication of AIE-based FNPs through controllable RAFT polymerization using a polymerizable AIE dye (A10) and a widely used

biomedical molecule (PEGMA) as monomers. The obtained copolymers with amphiphilic properties tended to self assemble into FNPs, with the AIE dye as the hydrophobic core and PEG as the hydrophilic shell. Due to the controllability and designability of RAFT polymerization, the obtained FNPs should be superior for practical biomedical applications.⁸⁷⁻⁸⁸

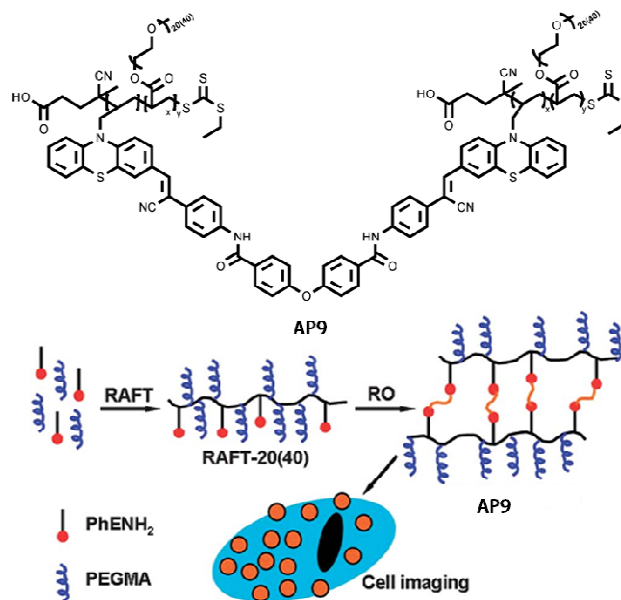


Figure 14 Chemical structure of AP9. Schematic showing the preparation of AP9 FNPs through RAFT polymerization and subsequent ring-opening (RO) condensation based on an AIE dye monomer (PhENH₂) and cell imaging applications of the thus obtained FNPs. (Reproduced from Ref. 89 with permission from Copyright 2014 The Royal Society of Chemistry).

Self-assembly of polymeric materials to form nanoscale structures such as spherical micelles or vesicles is a particularly promising strategy. However, such self-assembled structures are often unstable on dilute solution below the critical micelle concentration due to the poor intermolecular interactions of the non-crosslinked polymer. Thus the development of robust synthetic routes to novel stable cross-linked fluorescent polymeric nanoparticles is of considerable scientific interest. Wei's group (Fig. 14) reported a AIE-based stable cross linked polymer through RAFT polymerization and subsequent anhydride ring-opening polymerization, which are based on an AIE fluorogen monomer (PhENH₂) with one amino group, PEGMA and 4,4'-oxydiphthalic anhydride (OA)⁸⁹. Based on the designed degree of polymerization (DP), such obtained amphiphilic cross-linked copolymers AP9 are tended to self-assemble into stable FNPs with a diameter on the nanoscale and highly dispersed in aqueous solution. Incorporating the AIE fluorogen into copolymers through polymerization are expected to be more stable than surfactant-modified FNPs. Hereafter they have further developed some cross-linked strategy^{90, 91}. For example, through room temperature anhydride ring-opening polymerization based on 4,4'-oxydiphthalic anhydride (slight excess) and an AIE monomer (PhNH₂) with two amino end-groups under an air atmosphere,

a prepolymer was subsequently cross-linked with polyethylenimine or polyethylene polyamine to form the resulting cross-linked FNPs, which showed high dispersibility and strong red fluorescence in aqueous solution. Biocompatibility evaluation and cell imaging results suggested that these FNPs were biocompatible enough for bioimaging applications.

4 Fluorescent Silica Nanoparticles

Fluorescent Silica nanoparticles (FSNPs) have been shown to build up multimodality nanosystems. Silica is a non-toxic and biocompatible material⁹². It is "generally recognized as safe" (GRAS) by the US Food and Drug Administration (FDA), as demonstrated by its common usage in the food additives and vitamin supplements. Based on optical transparency and chemical inertness, FSNPs would be allowed doping with most of desired fluorophores (in both visible and near-infrared (NIR) region), which will lead to generate a series of imaging materials⁹³⁻⁹⁵. In addition, doped with bioactive molecules, such as enzymes, genetic materials, therapeutic drug molecules, FSNPs could be useful for specific biological applications.⁹⁶⁻⁹⁷ Furthermore, FSNPs also offers to easily achieve surface functionalization, which provide great opportunities to integrate additional functionalities, thus opening up new imaging and therapeutic avenues. There are two typical silica nanoparticles (SiNPs), silica physically encapsulated nanoparticles and covalent binding of silica nanoparticles.

4.1 Physically encapsulated AIE fluorogens silica nanoparticles

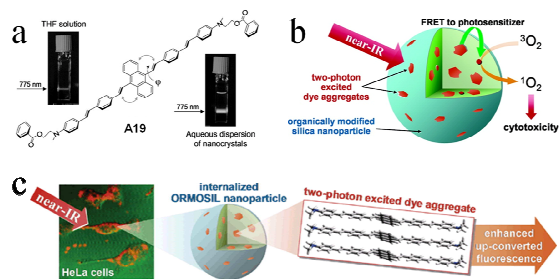


Figure 15 a) Chemical structure of A19 and the photographs show two-photon excited fluorescence of THF solution and nanocrystal dispersion stabilized in AOT/1-butanol/water at the same concentration (excited at 775 nm). b) scheme of two-photon photodynamic therapy with co-encapsulating photosensitizer drug and aggregation-enhanced two-photon absorbing fluorescent dye aggregates. c) scheme for the two-photon excited ORMOSIL nanoparticles used for near-IR cell imaging. (Reproduced from Ref. 98 with permission from Copyright 2007 Wiley-VCH & Reproduced from Ref. 99 with permission from Copyright 2007 American Chemical Society).

In 2007, Prasad and co-workers⁹⁸ developed a dye, 9,10-bis[4'-(4''-aminostyryl)styryl]anthracene derivative (A19), which has been shown to enhance one- and two-photon fluorescence without any intermolecular quenching effect (Fig. 15), which enables remarkable signal improvement by raising the A19 loading density in the composite nanoparticle. It has been shown by in-vitro cell experiments that the optimum loading level of A19, in terms of uptake

efficiency and intracellular fluorescence signal, which exists at around 30–40 wt % with respect to the organically modified silica (ORMOSIL) particle matrix. These A19/ORMOSIL composite nanoparticles were anticipated to provide a promising pathway to achieve a significant breakthrough in developing two-photon fluorescent probes for biomedical applications due to the advantages of two-photon properties, noninvasive cellular uptake and surface functionality for labeling. They also used energy-transferring organically modified silica nanoparticles to achieve two-photon photodynamic therapy.⁹⁹ These nanoparticles co-encapsulate a photosensitizing anticancer drug, HPPH, as an acceptor, and fluorescent aggregates of a two-photon absorbing dye, A19, as an energy up-converting donor. They combine aggregation-enhanced two-photon absorption and emission properties and FRET between nanoaggregate and a photosensitizer. The results show that these nanoparticles possess two advanced features. One is that the indirect excitation of the photosensitizer can be through efficient two-photon excited intraparticle energy transfer from the A19 aggregates in the intracellular environment of tumor cells. The other is that the generation of singlet oxygen in tumor cells by photosensitization can be observed under two-photon irradiation, and the nanoparticles also possess in vitro cytotoxic effect. It offered a simple and proper methodology for developing formulations of drug-carrier nanoassemblies applicable in two-photon activated PDT.

Moreover, a two-photon absorbing and aggregation-enhanced near-infrared emitting pyran derivative A16, which was encapsulated in silica nanoparticles, was reported by Belfield and co-workers¹⁰⁰ as a nanoscopic bioprobe for two-photon bioimaging. The new SiNPs probe exhibited aggregation-enhanced emission producing nearly twice as strong a signal as the unaggregated dye, a 3-fold increase in two-photon absorption relative to the A16 in solution, and approximately 4-fold increase in photostability. In order to specifically deliver the two-photon fluorescent SiNPs to a tumor, the surface of the nanoparticles was functionalized with PEG and then modified with a folic acid derivative at the outer terminus of the PEG group. These FR-targeting A16-encapsulating SiNPs were demonstrated as efficient probes for in vivo fluorescence bioimaging upon intravenous administration into mice bearing HeLa tumors. The real-time fluorescence image monitoring for the biodistribution of the SiNPs indicated that the SiNPs selectively accumulated in the tumor, most likely via FA-mediated active targeting.

In addition, Wei and co-workers¹⁰¹ introduced a one-pot surfactant templated method via facilely incorporating a distyrylanthracene derivative A13 with AIE features into mesoporous silica nanoparticles for cell imaging and cancer therapy applications. Qian's group also prepared the ORMOSIL nanoparticles encapsulated with the near-IR AIE molecular A6 for in vitro imaging of HeLa cells.¹⁰²

4.2 Covalent binding AIE fluorogens silica nanoparticles

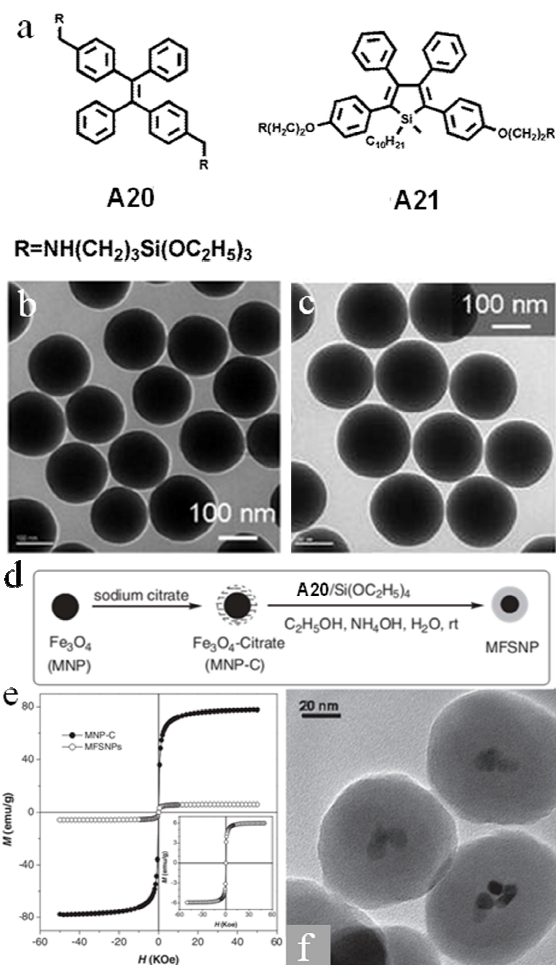


Figure 16 a) Chemical structures of A20 and A21. TEM images of monodispersed FSNP-1 b) and FSNP-2 c), d) Fabrication of A20-containing fluorescent magnetic silica nanoparticle MFSNP e) Plots of magnetization (M) versus applied magnetic field (H) at 300 K for MNP-C and MFSNPs. f) TEM images of MFSNPs. (Reproduced from Ref. 103&105 with permission from Copyright 2010 Wiley-VCH).

Despite the photobleaching resistance property and colloidal stability have been ameliorated, problems might occur that luminogens would leak out from the FSNPs, which would limit their practical bioimaging applications. Tang and co-workers¹⁰³ reported the first work on the syntheses of AIE-active FSNPs with core-shell structures through a surfactant-free sol-gel process in a one-pot experimental procedure. In this approach, the luminogens were chemically bound to, rather than physically blended with, the silica networks. The AIE fluorogens thus did not leak out from the FSNPs. Notably, the surfactant-free sol-gel reactions of TPE and silole functionalized siloxanes A20 and A21 (Fig 16) were carried out, and then subjected to further sol-gel reaction with tetraethylorthosilicate (TEOS) to afford fluorescent silica nanoparticles FSNP-1 and FSNP-2, respectively. The resultant FSNPs were mono-dispersed with smooth surfaces, which possessed strong fluorescence ($\Phi_f=30.1\%$ and 39%), high surface charges and excellent colloidal stability. Furthermore,

the particle diameters and emission efficiencies of the FSNPs could be manipulable by changing the reaction conditions and fluorogens loadings. The FSNPs showed low toxicity to living cells and could function as fluorescent visualizers for intracellular imaging. Covalent immobilization of AIE fluorogens in silica nanoparticles through click reaction has also been developed by one-pot, two-step Stober and reverse microemulsion techniques.¹⁰⁴

Multifunctional nanoparticles with both efficient fluorescence and strong magnetization (MFSNPs) are fabricated by one-pot, surfactant-free sol-gel reaction of tetraethoxysilane and silole-functionalized siloxane in the presence of citrate-coated magnetite nanoparticles (Fig 16d).¹⁰⁵ The MFSNPs are uniformly sized with smooth surfaces. They possess core-shell structures and exhibit appreciable surface charges and hence good colloidal stability. The MFSNPs are superparamagnetic, exhibiting no hysteresis at room temperature. (Fig 16e) The suspension of MFSNPs in ethanol gives strong green emission at 486 nm under UV irradiation, due to the AIE characteristics of the silole aggregates in the hybrid nanoparticles. The MFSNPs can selectively stain the cytoplasmic regions of the living cells and function as selective cell imaging bioprobes. These MFSNPs surfaces also can be readily modulated by varying the reactants. Addition of APS during the particle fabrication generates MFSNP-NH₂, which can serve as a protein carrier.

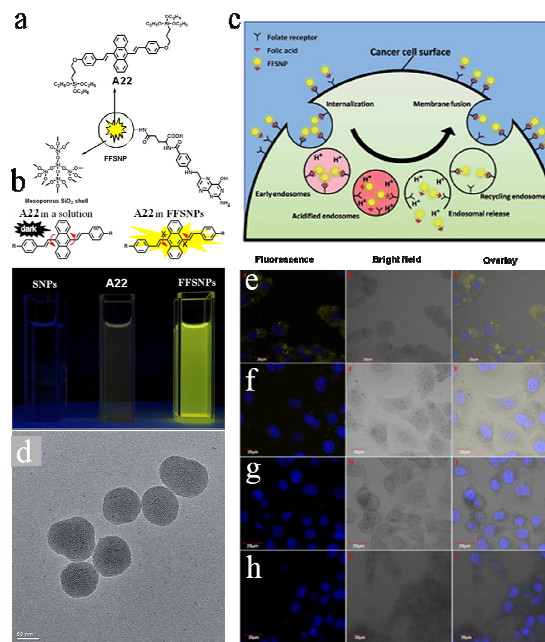


Figure 17 a) Scheme of FFSNPs. b) Solution and suspensions of A22, SNPs and FFSNPs in ethanol; photograph taken upon irradiation with a UV light of 365 nm. c) Folate-mediated delivery of FFSNPs to folate receptor-positive cancer cells. A fraction of the FFSNPs will traffic into the cancer cells by receptor-mediated endocytosis (left side of diagram), while the remainder will remain on the cell surfaces (right side of diagram), two types of strategies can be envisioned. d) TEM images of mono-dispersed FFSNPs. e) FFSNPs for HeLa. f) FFSNPs with free acid folic acid for HeLa. g) FFSNPs for HeLa. h) FFSNPs for 3T3-L1. (Reproduced from Ref. 107 with permission from Copyright 2012 The Royal Society of Chemistry).

In order to realize the specific living tumor cell imaging, the biotin-decorated FSNPs with strong light emissions in the solid state was fabricated. FSNP-1 was first decorated by (3-aminopropyl) triethoxysilane to generate FSNP-1-NH₂ with numerous amino groups decorated on the surface, enabling it to undergo amidation reaction with biotin in the presence of 1,3-dicyclohexylcarbodiimide and 4-(dimethylamino)pyridine to furnish FSNP-1-biotin.¹⁰⁶

In addition, our group has succeeded in designing and preparing highly emissive folate functionalized fluorescent silica nanoparticles (FFSNPs) with an AIE-active fluorogen A22 core and a folic acid-functionalized silica shell (Fig. 17a). Taken upon exposure to the irradiation under a UV light of 365 nm, the solution of A22 and the suspensions of SNPs almost have no light emission, and intense yellow light is emitted from FFSNPs (Fig. 17b). This visual observation further supports the idea that the intra-molecular rotations of A22 are restricted by the covalent melding of the AIE fluorogen with the silica matrix causing a burst in light emission. The resulting FFSNPs are monodispersed with a small size (60 nm), and high surface charges make FFSNPs stable in aqueous solution (Fig. 17d). The suspensions of FFSNPs emit strong yellow light upon photoexcitation, with a solid state fluorescence quantum yield up to 20%. FFSNPs are taken up nondestructively by mammalian cells via a specialized endocytosis pathway mediated by FR. With the folic acid-functionalized surface, FFSNPs should have a high binding affinity to FR. After binding to FR on the cancer cell surface, FFSNPs are seen to internalize and traffic to intracellular compartments called endosomes. (Fig. 17c) Moreover, the obtained FFSNPs show specific targeting ability to cancer cells (Fig. 17e) that overexpress the folate receptor, while avoiding normal cells (Fig. 17h) that do not overexpress this receptor. Taking into account the mesoporous structure of FFSNPs, encapsulating anticancer drugs to the FFSNPs could provide a promising material for cancer diagnosis and treatment.¹⁰⁷

Conclusions and Perspectives

This review summarized the recent development of fluorescent nanoparticles based on AIE fluorogens, which have provided a highly attractive platform for biological applications. For fluorescence bioimaging, the brightness, morphology, stability, toxicity and biocompatibility of FNPs. Thanks to the fantastic luminescent properties of AIE fluorogens¹⁰⁸, whose fluorescence is weak as isolate molecules but strong in aggregate state, they show great potential in fabricating highly fluorescent nanoparticles. A variety of AIE-based FNPs have been reported through many strategies¹⁰⁹, such as physical cladding AIE polymer nanoparticles, covalent AIE copolymer nanoparticles, and fluorescent silica nanoparticles. These FNPs possess many prominent advantages, for instance, uniform morphology, good biocompatibility, emission tunable from blue to NIR, highly fluorescent efficiency and various modification of surface functional groups. With the superiority of AIE-based FNPs, they have been demonstrated for targeted in vitro and in vivo tumor imaging, cancer cell tracing, specific

chemical and biomolecular species imaging, blood vessel imaging, and even organelle imaging.

FNPs based on AIE fluorogens are still a young field of research with numerous opportunities and challenges¹¹⁰. For instance, future work of AIE-based FNPs will be focused on developing novel FR/NIR AIE fluorogens with narrow band emission and high solid fluorescence quantum efficiency, which is benefit to weaken harmful effects on the biological samples and enhance the light penetrated length in vivo experiments. Exploring multifarious matrixes with good biocompatibility, stability and active surface groups for functional modification could be used to further improve performance and realize multifunctional composite of FNPs. In addition, combining with light, enzyme or pH responsive functional units to such highly emission FNPs will open new research area for bioimaging and sensing. This is a promising vista within the scope of AIE fluorogens. With these prospects, it is our expectations that this review can accelerate the development of these fascinating materials, with the new aspects of fluorescent properties, fabrication methodologies, novel and important function for biological applications.

Acknowledgements

This work was supported by 973 Program (2013CB834702), the Natural Science Foundation of China (No. 51373063, 21204027, 21221063) and and Program for Chang Jiang Scholars and Innovative Research Team in University (No. IRT101713018).

References

- 1 K. Kikuchi, *Chem. Soc. Rev.*, 2010, **39**, 2048-2053.
- 2 D. W. Domaille, E. L. Que and C. J. Chang, *Nat Chem Biol*, 2008, **4**, 168-175.
- 3 H. Kobayashi, M. Ogawa, R. Alford, P. L. Choyke and Y. Urano, *Chemical Reviews*, 2010, **110**, 2620-2640.
- 4 D. T. Quang and J. S. Kim, *Chemical Reviews*, 2010, **110**, 6280-6301.
- 5 A. Demchenko, *J Fluoresc*, 2010, **20**, 1099-1128.
- 6 D.-E. Lee, H. Koo, I.-C. Sun, J. H. Ryu, K. Kim and I. C. Kwon, *Chemical Society Reviews*, 2012, **41**, 2656-2672.
- 7 T. L. Doane and C. Burda, *Chemical Society Reviews*, 2012, **41**, 2885-2911.
- 8 R. Mout, D. F. Moyano, S. Rana and V. M. Rotello, *Chemical Society Reviews*, 2012, **41**, 2539-2544.
- 9 X. Zhang, S. Wang, M. Liu, B. Yang, L. Feng, Y. Ji, L. Tao and Y. Wei, *Physical Chemistry Chemical Physics*, 2013, **15**, 19013-19018.
- 10 X. Zhang, S. Wang, C. Zhu, M. Liu, Y. Ji, L. Feng, L. Tao and Y. Wei, *Journal of Colloid and Interface Science*, 2013, **397**, 39-44.
- 11 J. Hui, X. Zhang, Z. Zhang, S. Wang, L. Tao, Y. Wei and X. Wang, *Nanoscale*, 2012, **4**, 6967-6970.
- 12 X. Zhang, J. Hui, B. Yang, Y. Yang, D. Fan, M. Liu, L. Tao and Y. Wei, *Polymer Chemistry*, 2013, **4**, 4120-4125.
- 13 X. Wu, X. He, K. Wang, C. Xie, B. Zhou and Z. Qing, *Nanoscale*, 2010, **2**, 2244-2249.
- 14 A. Shiohara, S. Prabakar, A. Faramus, C.-Y. Hsu, P.-S. Lai, P. T. Northcote and R. D. Tilley, *Nanoscale*, 2011, **3**, 3364-3370.
- 15 J.-H. Kim, K. Park, H. Y. Nam, S. Lee, K. Kim and I. C. Kwon, *Progress in Polymer Science*, 2007, **32**, 1031-1053.

- 16 S. Song, Y. Qin, Y. He, Q. Huang, C. Fan and H.-Y. Chen, *Chemical Society Reviews*, 2010, **39**, 4234-4243.
- 17 Y. Wang, B. Yan and L. Chen, *Chemical Reviews*, 2013, **113**, 1391-1428.
- 18 V. Biju, *Chemical Society Reviews*, 2014, **43**, 744-764.
- 19 M. De, P. S. Ghosh and V. M. Rotello, *Advanced Materials*, 2008, **20**, 4225-4241.
- 20 M. Chen and M. Yin, *Progress in Polymer Science*, 2014, **39**, 365-395.
- 21 A. M. Smith, H. Duan, A. M. Mohs and S. Nie, *Advanced Drug Delivery Reviews*, 2008, **60**, 1226-1240.
- 22 J. P. Wilcoxon and B. L. Abrams, *Chemical Society Reviews*, 2006, **35**, 1162-1194.
- 23 F. Wang and X. Liu, *Chemical Society Reviews*, 2009, **38**, 976-989.
- 24 S. N. Baker and G. A. Baker, *Angewandte Chemie International Edition*, 2010, **49**, 6726-6744.
- 25 L. Wang, W. Zhao and W. Tan, *Nano Res.*, 2008, **1**, 99-115.
- 26 S. Luo, E. Zhang, Y. Su, T. Cheng and C. Shi, *Biomaterials*, 2011, **32**, 7127-7138.
- 27 J. Wu, W. Liu, J. Ge, H. Zhang and P. Wang, *Chemical Society Reviews*, 2011, **40**, 3483-3495.
- 28 J. O. Escobedo, O. Rusin, S. Lim and R. M. Strongin, *Current Opinion in Chemical Biology*, 2010, **14**, 64-70.
- 29 Z. Wang, S. Chen, J. W. Lam, W. Qin, R. T. Kwok, N. Xie, Q. Hu and B. Z. Tang, *J Am Chem Soc*, 2013, **135**, 8238-8245.
- 30 Y. Hong, J. W. Y. Lam and B. Z. Tang, *Chemical Society Reviews*, 2011, **40**, 5361-5388.
- 31 J. Luo, Z. Xie, J. W. Y. Lam, L. Cheng, H. Chen, C. Qiu, H. S. Kwok, X. Zhan, Y. Liu, D. Zhu and B. Z. Tang, *Chemical Communications*, 2001, 1740-1741.
- 32 Y. Liu, C. Deng, L. Tang, A. Qin, R. Hu, J. Z. Sun and B. Z. Tang, *Journal of the American Chemical Society*, 2011, **133**, 660-663.
- 33 J. Geng, K. Li, D. Ding, X. Zhang, W. Qin, J. Liu, B. Z. Tang and B. Liu, *Small*, 2012, **8**, 3655-3663.
- 34 S. Zhang, J. Yan, A. Qin, J. Sun and B. Tang, *Sci. China Chem.*, 2013, **56**, 1253-1257.
- 35 Q. Qi, X. Fang, Y. Liu, P. Zhou, Y. Zhang, B. Yang, W. Tian and S. X.-A. Zhang, *RSC Advances*, 2013, **3**, 16986-16989.
- 36 X. Xue, Y. Zhao, L. Dai, X. Zhang, X. Hao, C. Zhang, S. Huo, J. Liu, C. Liu, A. Kumar, W.-Q. Chen, G. Zou and X.-J. Liang, *Advanced Materials*, 2014, **26**, 712-717.
- 37 Z. Li, Y. Q. Dong, J. W. Y. Lam, J. Sun, A. Qin, M. H  u  ler, Y. P. Dong, H. H. Y. Sung, I. D. Williams, H. S. Kwok and B. Z. Tang, *Advanced Functional Materials*, 2009, **19**, 905-917.
- 38 Y. Dong, B. Xu, J. Zhang, X. Tan, L. Wang, J. Chen, H. Lv, S. Wen, B. Li, L. Ye, B. Zou and W. Tian, *Angewandte Chemie International Edition*, 2012, **51**, 10782-10785.
- 39 Y. Dong, J. Zhang, X. Tan, L. Wang, J. Chen, B. Li, L. Ye, B. Xu, B. Zou and W. Tian, *Journal of Materials Chemistry C*, 2013, **1**, 7554-7559.
- 40 J. He, B. Xu, F. Chen, H. Xia, K. Li, L. Ye and W. Tian, *The Journal of Physical Chemistry C*, 2009, **113**, 9892-9899.
- 41 X. Li, K. Ma, H. Lu, B. Xu, Z. Wang, Y. Zhang, Y. Gao, L. Yan and W. Tian, *Anal Bioanal Chem*, 2014, **406**, 851-858.
- 42 X. Li, K. Ma, S. Zhu, S. Yao, Z. Liu, B. Xu, B. Yang and W. Tian, *Analytical Chemistry*, 2014, **86**, 298-303.
- 43 X. Li, S. Zhu, B. Xu, K. Ma, J. Zhang, B. Yang and W. Tian, *Nanoscale*, 2013, **5**, 7776-7779.
- 44 H. Lu, B. Xu, Y. Dong, F. Chen, Y. Li, Z. Li, J. He, H. Li and W. Tian, *Langmuir*, 2010, **26**, 6838-6844.
- 45 H. Shi, J. Liu, J. Geng, B. Z. Tang and B. Liu, *Journal of the American Chemical Society*, 2012, **134**, 9569-9572.
- 46 B. Xu, J. Zhang, H. Fang, S. Ma, Q. Chen, H. Sun, C. Im and W. Tian, *Polymer Chemistry*, 2014, **5**, 479-488.
- 47 J. Zhang, J. Chen, B. Xu, L. Wang, S. Ma, Y. Dong, B. Li, L. Ye and W. Tian, *Chemical Communications*, 2013, **49**, 3878-3880.
- 48 B. Sezen, R. Franz and D. Sames, *Journal of the American Chemical Society*, 2006, **128**, 8364-8364.
- 49 X. Y. Shen, W. Z. Yuan, Y. Liu, Q. Zhao, P. Lu, Y. Ma, I. D. Williams, A. Qin, J. Z. Sun and B. Z. Tang, *The Journal of Physical Chemistry C*, 2012, **116**, 10541-10547.
- 50 K. Li, Y. Jiang, D. Ding, X. Zhang, Y. Liu, J. Hua, S. S. Feng and B. Liu, *Chem Commun (Camb)*, 2011, **47**, 7323-7325.
- 51 D. Wang, J. Qian, S. He, J. S. Park, K. S. Lee, S. Han and Y. Mu, *Biomaterials*, 2011, **32**, 5880-5888.
- 52 Z. Zhao, J. Geng, Z. Chang, S. Chen, C. Deng, T. Jiang, W. Qin, J. W. Y. Lam, H. S. Kwok, H. Qiu, B. Liu and B. Z. Tang, *Journal of Materials Chemistry*, 2012, **22**, 11018.
- 53 Q. Zhao, K. Li, S. Chen, A. Qin, D. Ding, S. Zhang, Y. Liu, B. Liu, J. Z. Sun and B. Z. Tang, *Journal of Materials Chemistry*, 2012, **22**, 15128.
- 54 J. Geng, K. Li, D. Ding, X. Zhang, W. Qin, J. Liu, B. Z. Tang and B. Liu, *Small*, 2012, **8**, 3655-3663.
- 55 J. Geng, Z. Zhu, W. Qin, L. Ma, Y. Hu, G. G. Gurzadyan, B. Z. Tang and B. Liu, *Nanoscale*, 2014, **6**, 939-945.
- 56 K. Li, W. Qin, D. Ding, N. Tomczak, J. Geng, R. Liu, J. Liu, X. Zhang, H. Liu, B. Liu and B. Z. Tang, *Scientific reports*, 2013, **3**, 1150.
- 57 G. Feng, C. Y. Tay, Q. X. Chui, R. Liu, N. Tomczak, J. Liu, B. Z. Tang, D. T. Leong and B. Liu, *Biomaterials*, 2014, **35**, 8669-8677.
- 58 W. Qin, K. Li, G. Feng, M. Li, Z. Yang, B. Liu and B. Z. Tang, *Advanced Functional Materials*, 2014, **24**, 635-643.
- 59 K. Li, Z. Zhu, P. Cai, R. Liu, N. Tomczak, D. Ding, J. Liu, W. Qin, Z. Zhao, Y. Hu, X. Chen, B. Z. Tang and B. Liu, *Chemistry of Materials*, 2013, **25**, 4181-4187.
- 60 K. Li, D. Ding, C. Prashant, W. Qin, C. T. Yang, B. Z. Tang and B. Liu, *Advanced healthcare materials*, 2013, **2**, 1600-1605.
- 61 J. Qian, Z. Zhu, A. Qin, W. Qin, L. Chu, F. Cai, H. Zhang, Q. Wu, R. Hu, B. Z. Tang and S. He, *Adv Mater*, 2015, **27**, 2332-2339.
- 62 D. Ding, C. C. Goh, G. Feng, Z. Zhao, J. Liu, R. Liu, N. Tomczak, J. Geng, B. Z. Tang, L. G. Ng and B. Liu, *Adv Mater*, 2013, **25**, 6083-6088.
- 63 Z. Zhao, B. Chen, J. Geng, Z. Chang, L. Aparicio-Ixta, H. Nie, C. C. Goh, L. G. Ng, A. Qin, G. Ramos-Ortiz, B. Liu and B. Z. Tang, *Particle & Particle Systems Characterization*, 2014, **31**, 481-491.
- 64 D. Wang, J. Qian, W. Qin, A. Qin, B. Z. Tang and S. He, *Scientific reports*, 2014, **4**, 4279.
- 65 K. Li, M. Yamamoto, S. J. Chan, M. Y. Chiam, W. Qin, P. T. Wong, E. K. Yim, B. Z. Tang and B. Liu, *Chem Commun (Camb)*, 2014, **50**, 15136-15139.
- 66 D. Ding, D. Mao, K. Li, X. Wang, W. Qin, R. Liu, D. S. Chiam, N. Tomczak, Z. Yang, B. Z. Tang, D. Kong and B. Liu, *ACS Nano*, 2014, **8**, 12620-12631.
- 67 W.-C. Wu, C.-Y. Chen, Y. Tian, S.-H. Jang, Y. Hong, Y. Liu, R. Hu, B. Z. Tang, Y.-T. Lee, C.-T. Chen, W.-C. Chen and A. K. Y. Jen, *Advanced Functional Materials*, 2010, **20**, 1413-1423.
- 68 X. Zhang, X. Zhang, S. Wang, M. Liu, L. Tao and Y. Wei, *Nanoscale*, 2013, **5**, 147-150.
- 69 H. Lu, X. Zhao, W. Tian, Q. Wang and J. Shi, *RSC Advances*, 2014, **4**, 18460.
- 70 Z. Wang, L. Yan, L. Zhang, Y. Chen, H. Li, J. Zhang, Y. Zhang, X. Li, B. Xu, X. Fu, Z. Sun and W. Tian, *Polym. Chem.*, 2014, **5**, 7013-7020.
- 71 W. Qin, D. Ding, J. Liu, W. Z. Yuan, Y. Hu, B. Liu and B. Z. Tang, *Advanced Functional Materials*, 2012, **22**, 771-779.
- 72 D. Ding, K. Li, W. Qin, R. Zhan, Y. Hu, J. Liu, B. Z. Tang and B. Liu, *Advanced healthcare materials*, 2013, **2**, 500-507.
- 73 Y. Zhang, K. Chang, B. Xu, J. Chen, L. Yan, S. Ma, C. Wu and W. Tian, *RSC Advances*, 2015, **5**, 36837-36844.

- 74 M. Li, Y. Hong, Z. Wang, S. Chen, M. Gao, R. T. Kwok, W. Qin, J. W. Lam, Q. Zheng and B. Z. Tang, *Macromol Rapid Commun*, 2013, **34**, 767-771.
- 75 D. Ding, R. T. K. Kwok, Y. Yuan, G. Feng, B. Z. Tang and B. Liu, *Mater. Horiz.*, 2015, **2**, 100-105.
- 76 X. Zhang, X. Zhang, B. Yang, M. Liu, W. Liu, Y. Chen and Y. Wei, *Polymer Chemistry*, 2013, **4**, 4317.
- 77 C. Niu, Q. Liu, Z. Shang, L. Zhao and J. Ouyang, *Nanoscale*, 2015, **7**, 8457-8465.
- 78 Z. Huang, X. Zhang, X. Zhang, C. Fu, K. Wang, J. Yuan, L. Tao and Y. Wei, *Polym. Chem.*, 2015, **6**, 607-612.
- 79 C. Zhang, S. Jin, S. Li, X. Xue, J. Liu, Y. Huang, Y. Jiang, W. Q. Chen, G. Zou and X. J. Liang, *ACS applied materials & interfaces*, 2014, **6**, 5212-5220.
- 80 X. Zhang, X. Zhang, B. Yang, L. Liu, F. Deng, J. Hui, M. Liu, Y. Chen and Y. Wei, *RSC Advances*, 2014, **4**, 24189.
- 81 Y. Zhang, Y. Chen, X. Li, J. Zhang, J. Chen, B. Xu, X. Fu and W. Tian, *Polymer Chemistry*, 2014, **5**, 3824.
- 82 X. Zhang, X. Zhang, B. Yang, M. Liu, W. Liu, Y. Chen and Y. Wei, *Polym. Chem.*, 2014, **5**, 399-404.
- 83 H. Lu, F. Su, Q. Mei, Y. Tian, W. Tian, R. H. Johnson and D. R. Meldrum, *J Mater Chem*, 2012, **22**, 9890-9900.
- 84 H. Lu, F. Su, Q. Mei, X. Zhou, Y. Tian, W. Tian, R. H. Johnson and D. R. Meldrum, *Journal of polymer science. Part A, Polymer chemistry*, 2012, **50**, 890-899.
- 85 C. Ma, Q. Ling, S. Xu, H. Zhu, G. Zhang, X. Zhou, Z. Chi, S. Liu, Y. Zhang and J. Xu, *Macromolecular bioscience*, 2014, **14**, 235-243.
- 86 X. Zhang, X. Zhang, B. Yang, M. Liu, W. Liu, Y. Chen and Y. Wei, *Polym. Chem.*, 2014, **5**, 356-360.
- 87 X. Zhang, X. Zhang, K. Wang, H. Liu, Z. Gu, Y. Yang and Y. Wei, *J. Mater. Chem. C*, 2015, **3**, 1738-1744.
- 88 K. Wang, X. Zhang, X. Zhang, B. Yang, Z. Li, Q. Zhang, Z. Huang and Y. Wei, *Macromolecular Chemistry and Physics*, 2015, **216**, 678-684.
- 89 X. Zhang, X. Zhang, B. Yang, J. Hui, M. Liu, Z. Chi, S. Liu, J. Xu and Y. Wei, *Polym. Chem.*, 2014, **5**, 683-688.
- 90 X. Zhang, X. Zhang, B. Yang, J. Hui, M. Liu, Z. Chi, S. Liu, J. Xu and Y. Wei, *J. Mater. Chem. C*, 2014, **2**, 816-820.
- 91 X. Zhang, X. Zhang, B. Yang, J. Hui, M. Liu and Y. Wei, *Colloids and surfaces. B, Biointerfaces*, 2014, **116**, 739-744.
- 92 X. W. Lou, L. A. Archer and Z. Yang, *Advanced Materials*, 2008, **20**, 3987-4019.
- 93 T. J. Brunner, P. Wick, P. Manser, P. Spohn, R. N. Grass, L. K. Limbach, A. Bruinink and W. J. Stark, *Environmental Science & Technology*, 2006, **40**, 4374-4381.
- 94 H. Ow, D. R. Larson, M. Srivastava, B. A. Baird, W. W. Webb and U. Wiesner, *Nano Letters*, 2005, **5**, 113-117.
- 95 X. Zhao, R. Tapecc-Dytioco and W. Tan, *Journal of the American Chemical Society*, 2003, **125**, 11474-11475.
- 96 T. K. Jain, I. Roy, T. K. De and A. Maitra, *Journal of the American Chemical Society*, 1998, **120**, 11092-11095.
- 97 X. Fang, X. Liu, S. Schuster and W. Tan, *Journal of the American Chemical Society*, 1999, **121**, 2921-2922.
- 98 S. Kim, H. E. Pudavar, A. Bonoiu and P. N. Prasad, *Advanced Materials*, 2007, **19**, 3791-3795.
- 99 S. Kim, T. Y. Ohulchanskyy, H. E. Pudavar, R. K. Pandey and P. N. Prasad, *Journal of the American Chemical Society*, 2007, **129**, 2669-2675.
- 100 X. Wang, A. R. Morales, T. Urakami, L. Zhang, M. V. Bondar, M. Komatsu and K. D. Belfield, *Bioconjugate chemistry*, 2011, **22**, 1438-1450.
- 101 X. Zhang, X. Zhang, S. Wang, M. Liu, Y. Zhang, L. Tao and Y. Wei, *ACS applied materials & interfaces*, 2013, **5**, 1943-1947.
- 102 Z. Zhu, X. Zhao, W. Qin, G. Chen, J. Qian and Z. Xu, *Sci. China Chem.*, 2013, **56**, 1247-1252.
- 103 M. Faisal, Y. Hong, J. Liu, Y. Yu, J. W. Lam, A. Qin, P. Lu and B. Z. Tang, *Chemistry*, 2010, **16**, 4266-4272.
- 104 F. Mahtab, J. W. Lam, Y. Yu, J. Liu, W. Yuan, P. Lu and B. Z. Tang, *Small*, 2011, **7**, 1448-1455.
- 105 F. Mahtab, Y. Yu, J. W. Y. Lam, J. Liu, B. Zhang, P. Lu, X. Zhang and B. Z. Tang, *Advanced Functional Materials*, 2011, **21**, 1733-1740.
- 106 M. Li, J. W. Y. Lam, F. Mahtab, S. Chen, W. Zhang, Y. Hong, J. Xiong, Q. Zheng and B. Z. Tang, *J. Mater. Chem. B*, 2013, **1**, 676-684.
- 107 Z. Wang, B. Xu, L. Zhang, J. Zhang, T. Ma, J. Zhang, X. Fu and W. Tian, *Nanoscale*, 2013, **5**, 2065-2072.
- 108 R. Hu, N. L. Leung and B. Z. Tang, *Chem Soc Rev*, 2014, **43**, 4494-4562.
- 109 X. Zhang, X. Zhang, L. Tao, Z. Chi, J. Xu and Y. Wei, *Journal of Materials Chemistry B*, 2014, **2**, 4398.
- 110 K. Li and B. Liu, *Chem Soc Rev*, 2014, **43**, 6570-6597.